



Deposited via The University of Leeds.

White Rose Research Online URL for this paper:

<https://eprints.whiterose.ac.uk/id/eprint/129943/>

Version: Accepted Version

Article:

Yan, S, Boyanov, MI, Mishra, B et al. (2018) U(VI) Reduction by Biogenic and Abiotic Hydroxycarbonate Green Rusts: Impacts on U(IV) Speciation and Stability Over Time. *Environmental science & technology*, 52. pp. 4601-4609. ISSN: 0013-936X

<https://doi.org/10.1021/acs.est.7b06405>

(c) 2018 American Chemical Society. This document is the Accepted Manuscript version of a Published Work that appeared in final form in *Environmental Science and Technology* after peer review and technical editing by the publisher. To access the final edited and published work see <https://doi.org/10.1021/acs.est.7b06405>

Reuse

Items deposited in White Rose Research Online are protected by copyright, with all rights reserved unless indicated otherwise. They may be downloaded and/or printed for private study, or other acts as permitted by national copyright laws. The publisher or other rights holders may allow further reproduction and re-use of the full text version. This is indicated by the licence information on the White Rose Research Online record for the item.

Takedown

If you consider content in White Rose Research Online to be in breach of UK law, please notify us by emailing eprints@whiterose.ac.uk including the URL of the record and the reason for the withdrawal request.

Supporting Information

U(VI) Reduction by Biogenic and Abiotic Hydroxycarbonate Green Rusts: Impacts on U(IV) Speciation and Stability Over Time

Sen Yan,^{1,2*} Maxim I. Boyanov,^{2,3} Bhoopesh Mishra,^{2,4} Kenneth M. Kemner,² and
Edward J. O'Loughlin^{2*}

1. School of Earth Sciences, China University of Geosciences, Wuhan, China

(sen.yan@cug.edu.cn)

2. Biosciences Division, Argonne National Laboratory, Argonne, IL, USA

(kemner@anl.gov, oloughlin@anl.gov)

3. Institute of Chemical Engineering, Bulgarian Academy of Sciences, Sofia, Bulgaria

(mboyanov@ice.bas.bg)

4. School of Chemical and Process Engineering, University of Leeds, Leeds, UK

(b.mishra@leeds.ac.uk)

Number of pages: 13; Number of Tables: 2; Number of Figures: 11

* Corresponding author (SY) phone: (86) 27-67883033; e-mail: sen.yan@cug.edu.cn; address: School of Earth Sciences, China University of Geosciences, 388 Lumo Road, Wuhan, China, 430074.

* Corresponding author (EJO) phone: (630) 252-9902; e-mail: oloughlin@anl.gov. Corresponding author address: Biosciences Division, Argonne National Laboratory, Building 203, Room E-137, 9700 South Cass Ave., Argonne, IL 60439-4843.

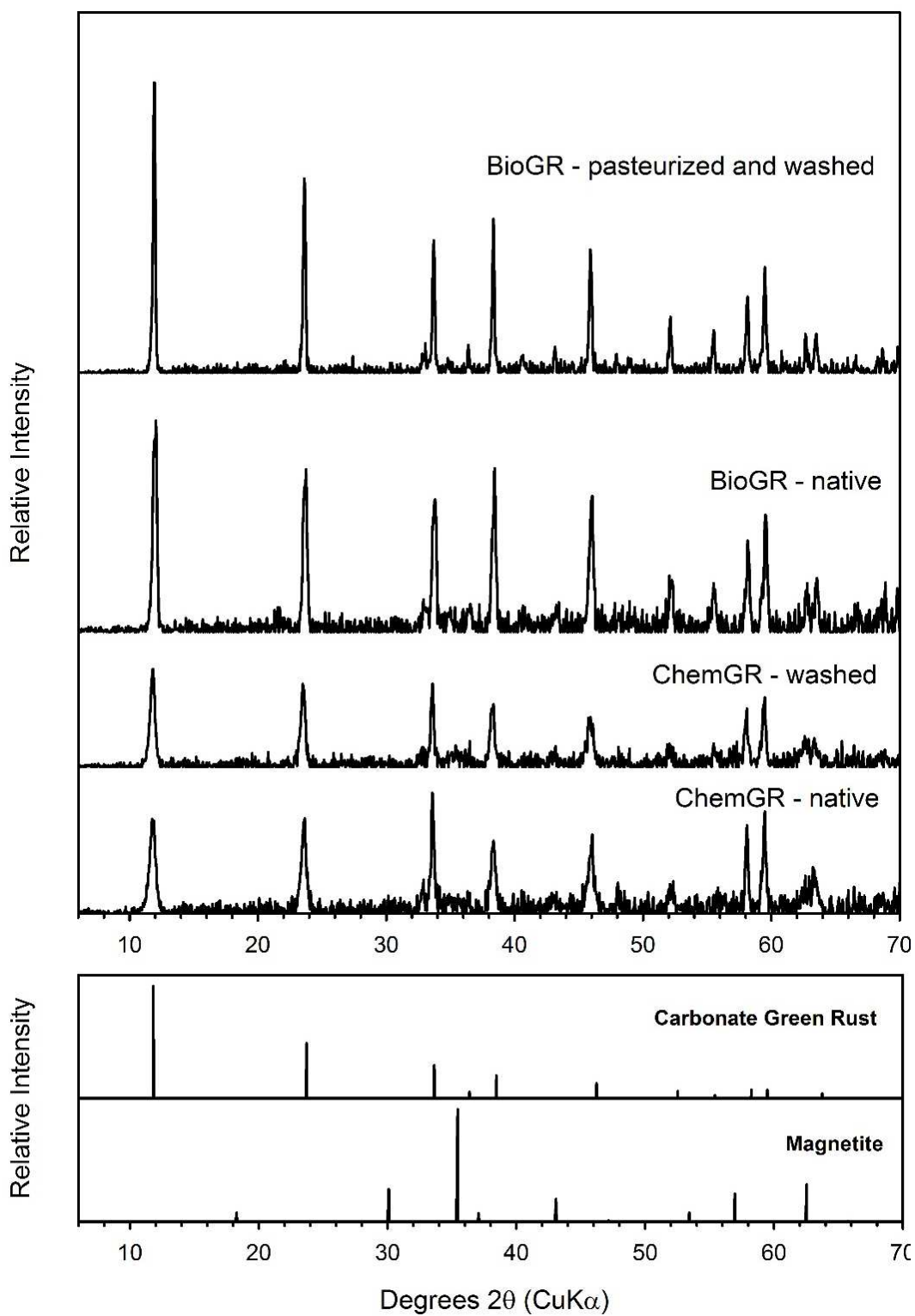


Figure S1. pXRD patterns of ChemGR before and after washing and BioGR before and after pasteurization (65 °C for 1 h) and washing.

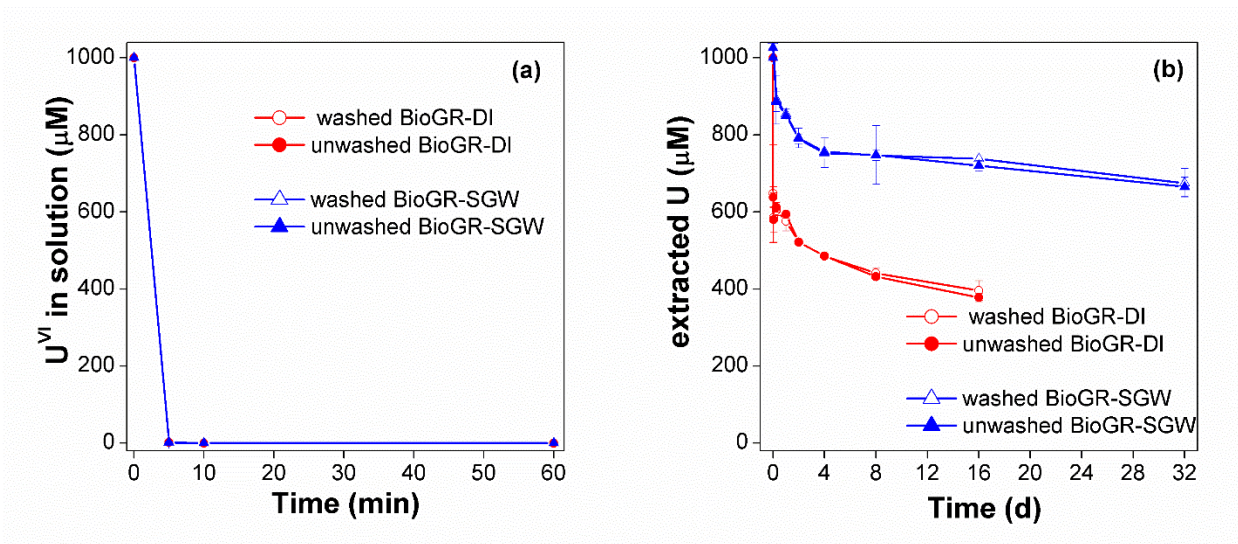


Figure S2. U^{VI} removal (a) and U extraction (b) in the systems with washed and unwashed BioGR.

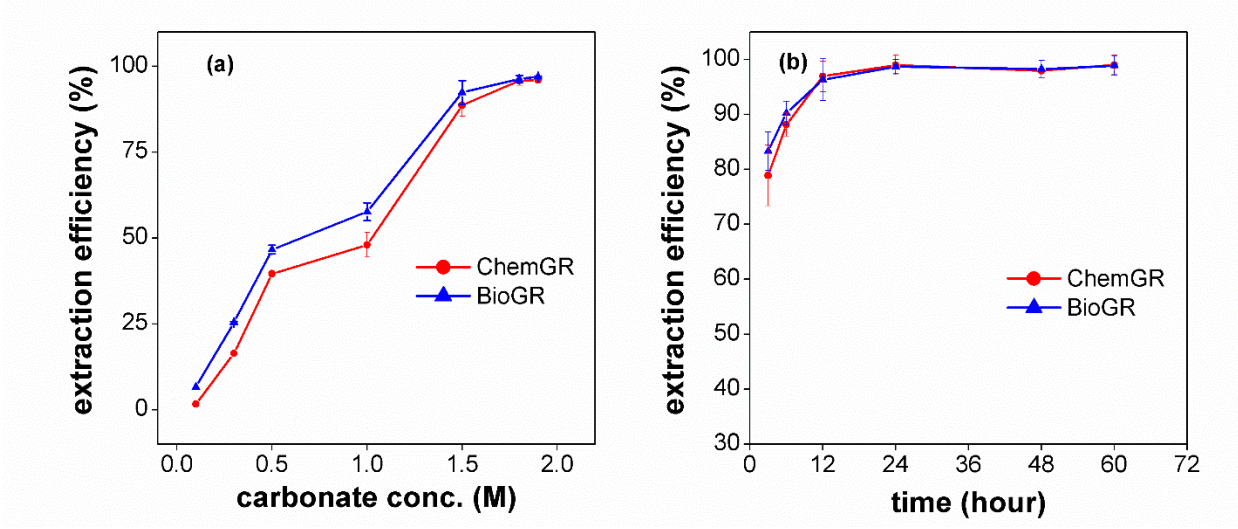


Figure S3. The effects of carbonate concentration (a) and time (b) on U extraction efficiency.

XAFS Data Collection and Analysis

U L_{III} edge (17,166 eV) x-ray absorption spectroscopy measurements were carried out at the MRCAT/EnviroCAT insertion device beamline (Sector 10-ID, Advanced Photon Source).¹ Fluorescence-mode x-ray absorption near edge spectra (XANES) and extended x-ray absorption fine structure (EXAFS) spectra were collected using an Ar-filled ionization chamber. Solution samples were loaded in 3-mm-thick sample holders sealed with x-ray transparent Kapton windows. The reactor solids from the GR systems were collected by filtration through a 0.22- μ m filter membrane inside an anoxic glovebox (Coy technologies, 5% H_2 /95% N_2 , Pd catalyst; O_2 in the gas environment <1 ppm at all times). The hydrated solids were covered with Kapton film, then sealed within two pieces of Kapton tape for the x-ray measurement. All samples were transported in O_2 -free containers to the beamline nearby. Spectra were collected at room temperature inside a N_2 -purged sample cell. Radiation-induced changes in U speciation were not observed in quick XANES scans (<30 sec each) on a fresh area of the samples. No differences were observed between spectra collected from several different areas on the sample. Therefore, all scans were combined to produce the final spectrum from each sample. Standards used in the analysis were collected at the same beamline during previous beam runs. Beamline energy calibration was maintained by measurements of spectra from a stable reference (hydrogen uranyl phosphate) simultaneously with the collection of data from the experimental samples.

Analysis of the experimental spectra involved comparisons to standards. Then the data were numerically modelled to extract the structural parameters that describe the average atomic coordination around U. Valence state references included a sample of U^{VI} adsorbed to goethite, a nanoparticulate uraninite U^{IV} standard that was synthesized and characterized in previous work,² and a U^{IV} -carbonate complex. The U^{IV} -carbonate complex spectrum used to represent the complex in the LCF analysis was not obtained from a U^{IV} -carbonate reference compound, but from solid-phase U^{IV} produced by the reduction of U^{VI} by either bacteria or abiotically by 9,10-anthrahydroquinone-2,6-disulfonate (AH_2DS) in 30 mM bicarbonate media.³ Normalization and background removal of the data were done using the program AUTOBK.⁴ The numerical

analysis of the spectra are based on the crystal structure of uraninite.⁵ The code FEFF8⁶ was used to generate the single-scattering contributions in the EXAFS for the O and U coordination shells in uraninite. Refinement of the numerical parameters against the experimental data was done in R-space using the program FEFFIT.⁷

The EXAFS data obtained from the BioGR system were best fit with a model consisting of an O, Fe, and O shell. The data were Fourier transformed at k^1 , k^2 , and k^3 weights ($FT[\chi(k)*k^n]$) and the three functions were fit simultaneously in R-space with the same fitting parameters. The purpose of multiple k-weight fitting is to provide additional contrast between light (e.g. O, C) and heavy (e.g. Fe) element contributions in the spectra, as the two generally have different amplitude dependencies with increasing k-values. By emphasizing the lower- or higher-k part of the spectrum using k^n -weighting, the relative proportion of light and heavy element contributions in the FT spectrum is changed (see orange and cyan lines in Figure S10), so if a heavy element contribution is fit with a light element shell there will be a misfit. The best fit for our data at all k-weights was obtained with a model consisting of an O, Fe, and O shell, as shown in Figure S10 and Table S2. The inclusion of the outer O shell in the EXAFS model was warranted because a fit without this shell resulted in a 5.7 fold increase of the reduced- χ^2 value of the fit (Table S2). It is possible that the signal fit by this shell is resulting from O atoms from farther binding sites on the surface of GR. However, fits of outer-shell EXAFS data are, in general, uncertain due to the potential contributions of multiple-scattering effects and/or an increased number of overlapping signals from several coordinating shells as the radial distance from the studied atom is increased. The data here do not allow differentiation between these signals, so we are modelling their aggregate contribution in the experimental spectrum as a single O shell with a resulting large coordination number and large disorder (i.e., Debye-Waller factor). The main purpose of the fit in Figure S10 is to determine the contribution of the closer Fe shell (at $\sim 3 \text{ \AA}$), the presence of which is interpreted as an indication of the U^{IV} adsorption complex at the GR surface. Thus, determining the exact origin of the signals modelled here by the 3rd coordination shell is not critical, but the presence of this signal in the fit is needed to produce a “background” or “overlap” contribution for the fit of the

neighboring shells. As can be seen from Table S2, the fit parameters for the Fe shell are not significantly affected by the presence or absence of the outer O shell.

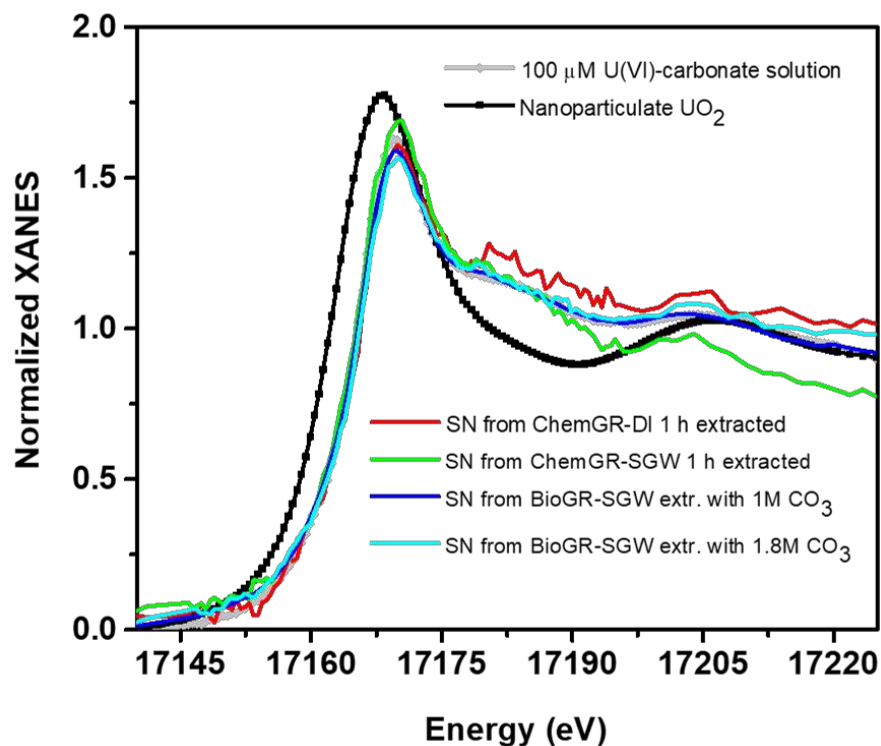


Figure S4. Comparisons of the XANES data from the carbonate extraction supernatants (SN) of the ChemGR and BioGR systems to the data from a 100 μM U^{VI} -carbonate solution standard and a nanoparticulate uraninite standard. The data overlay the U^{VI} standard, indicating that U^{VI} predominates in the extract solution.

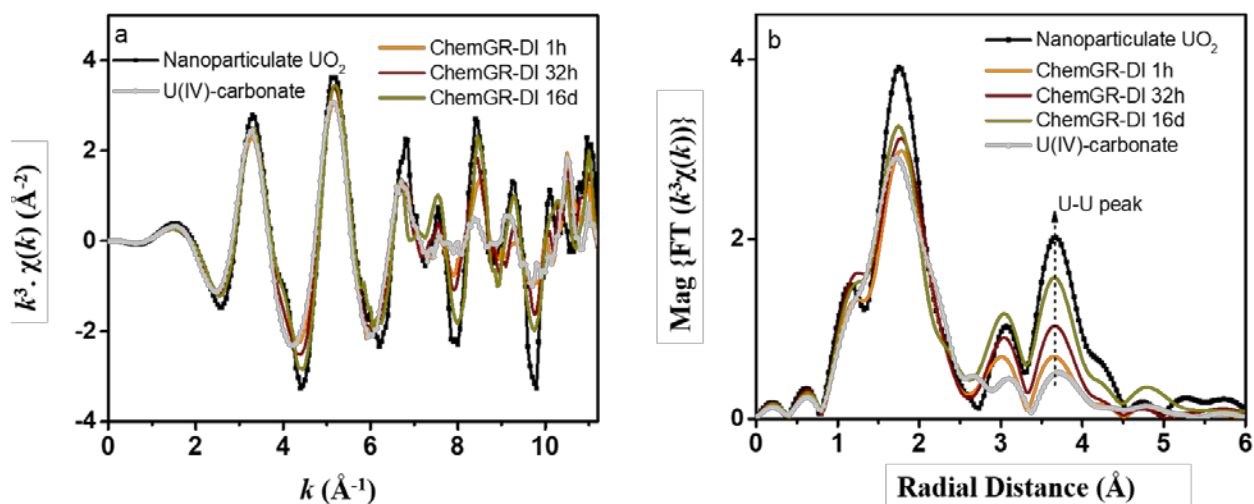


Figure S5. (a) k^3 -weighted $\chi(k)$ EXAFS data and (b) Fourier transformed EXAFS data for ChemGR in DI-water system after 1 h, 32 h, and 16 d, plotted with nanoparticulate uraninite and U^{IV} -carbonate standards. The vertical dashed line indicates the peak in the FT EXAFS data resulting from the contribution of the U shell in uraninite. The Fourier transform is within the data range $k = 2.2\text{--}10.4 \text{ \AA}^{-1}$ using $1.0\text{-}\text{\AA}^{-1}$ -wide Hanning windowsills.

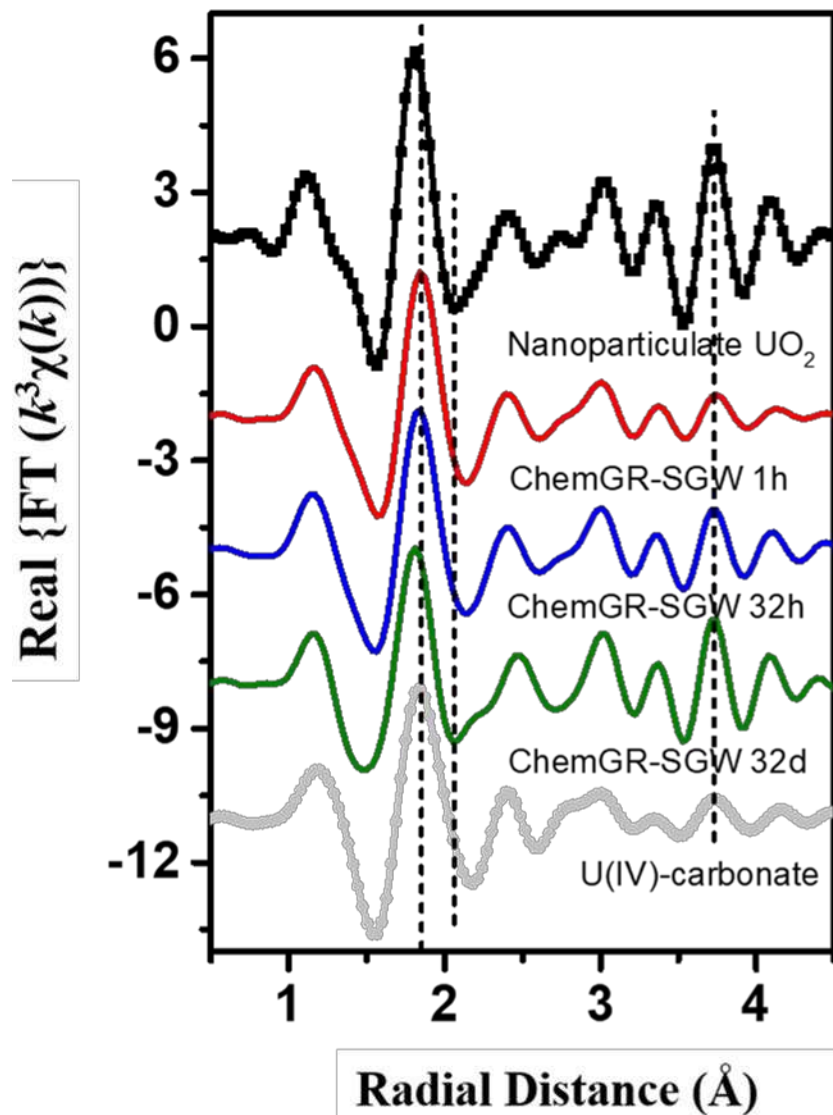


Figure S6. Real part of the Fourier transformed EXAFS data for ChemGR in the SGW system after 1 h, 32 h, and 32 d plotted with nanoparticulate uraninite and U^{IV}-carbonate standards. The vertical lines are guides to the eye for the positions of the different features. The lines at 1.8 Å and 2.1 Å correspond to the contribution of the O shell. The line at 3.7 Å corresponds to the contribution of the U shell in uraninite. The features at these positions show similarity of the 1-h sample to the U^{IV}-carbonate standard, whereas the 32-d sample is more similar to uraninite.

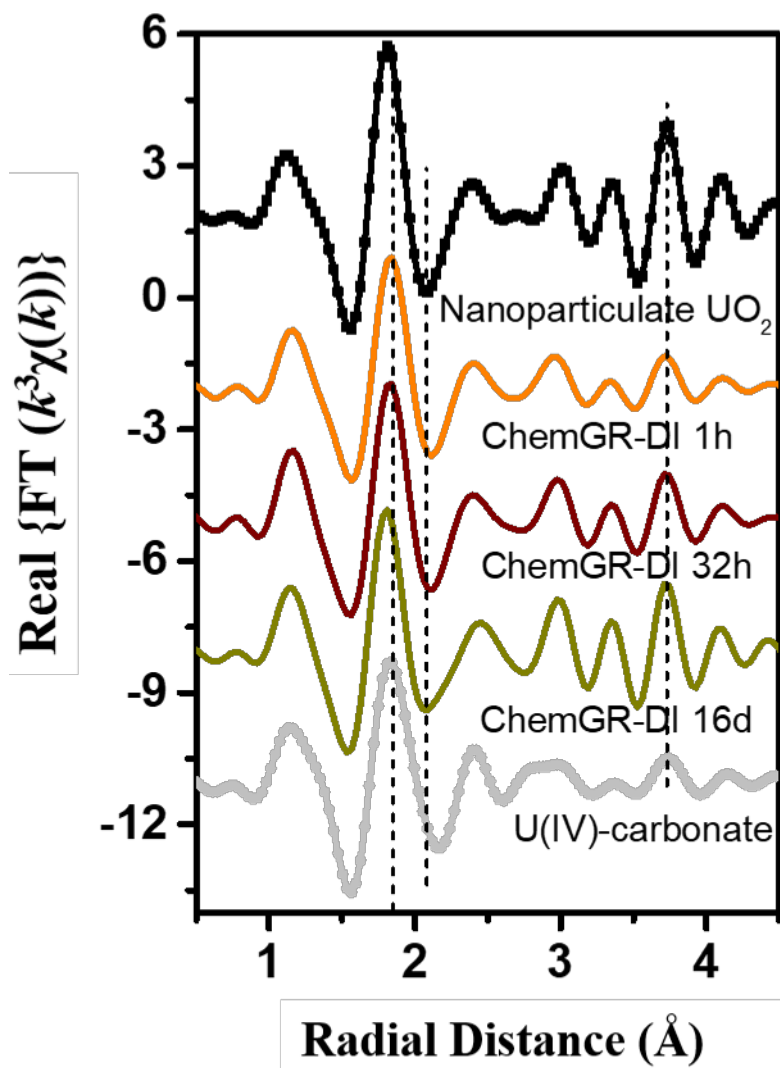


Figure S7. Real part of the Fourier transformed EXAFS data for the ChemGR system in the DI-water after 1 h, 32 h, and 16 d, plotted with nanoparticulate uraninite and U^{IV} -carbonate standards. The vertical lines are guides to the eye for the positions of the different features. The lines at 1.8 Å and 2.1 Å correspond to the contribution of the O shell, whereas the line at 3.7 Å corresponds to the contribution of the U shell in uraninite. The features at these positions show similarity of the 1-h sample to the U^{IV} -carbonate standard, whereas the 32-d sample is more similar to uraninite.

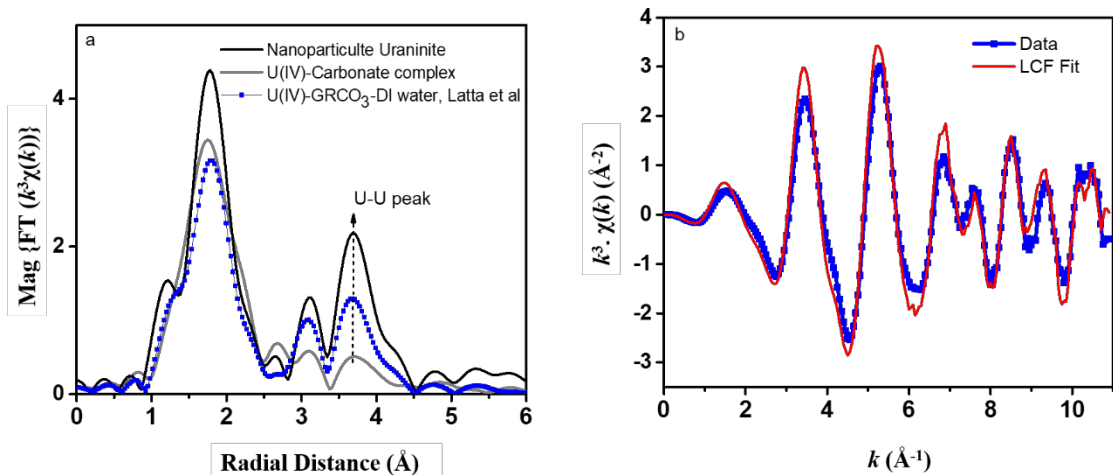


Figure S8. (a) Comparisons between the Fourier transformed EXAFS data from the 4-d ChemGR reactor with DI water in the study of Latta et al.⁸ (symbols) to the nanoparticulate uraninite standard (black) and the carbonate-complexed U^{IV} spectrum (grey), both from Boyanov et al.³ The Fourier transform is between $k = 2.2\text{--}10.4 \text{ \AA}^{-1}$. The vertical dashed line highlights the region where the U shell in uraninite contributes. Right: Linear combination fit between $k = 2.2\text{--}10.4 \text{ \AA}^{-1}$ of the $k^3\chi(k)$ data in Latta et al.⁸ with the standards described above. The refined spectral proportions are 58% nanoparticulate uraninite and 42% carbonate-complexed U^{IV}.

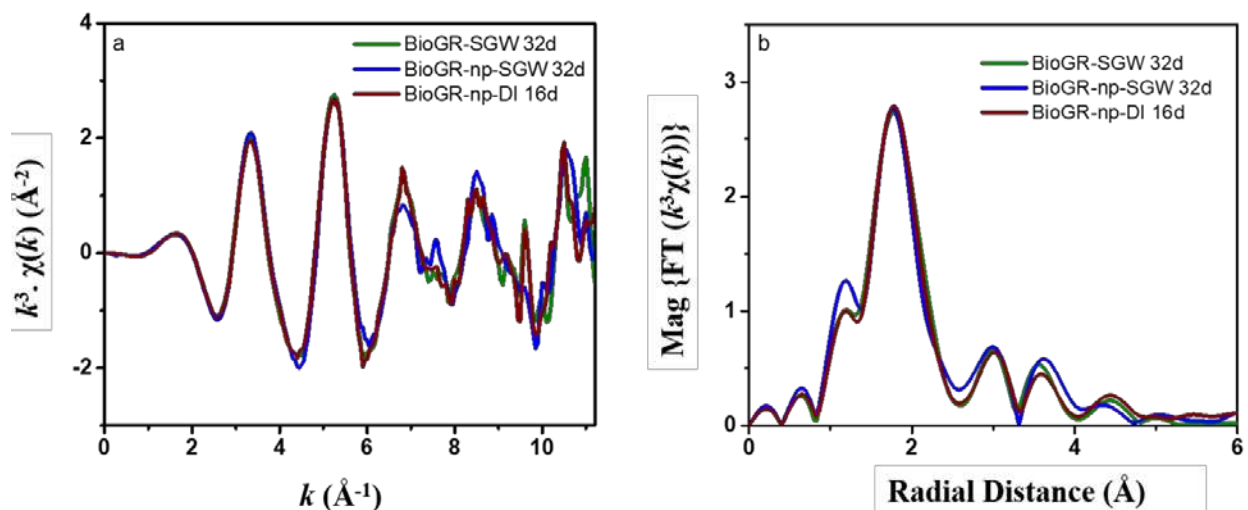


Figure S9. U L_{III} edge (a) k^3 -weighted $\chi(k)$ EXAFS data and (b) Fourier-transformed EXAFS data for BioGR in the DI-water and SGW systems (np means the non-pasteurized samples).

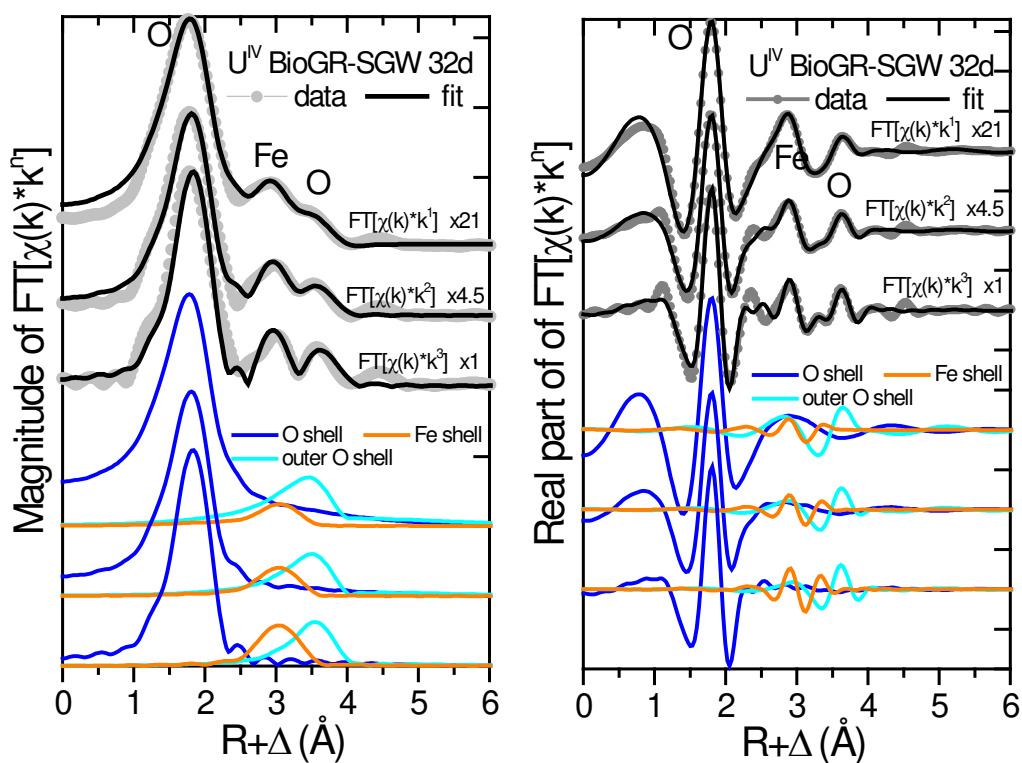


Figure S10. Best fit (line) of the BioGR EXAFS data (symbols) with a model consisting of an O, Fe, and O shell, as discussed in the text. The EXAFS data from the BioGR sample are Fourier transformed at k^1 , k^2 , and k^3 weight ($FT[\chi(k)*k^n]$) and the three functions are fit simultaneously in R-space with the same fitting parameters shown in Table S2. The scaling factors shown to the right of each graph are applied to both data and fit for better presentation of the three sets on the same graph. The scaled individual contributions of each shell are illustrated below in colored lines for the corresponding k-weight of the FT (note that the individual contributions combine linearly only in the real part of the FT to produce the fit line, not in the magnitude). The Fourier transforms are between $k=2.2 - 10.4 \text{ \AA}^{-1}$, fits are between $R+\Delta = 1.5 - 4.0 \text{ \AA}$.

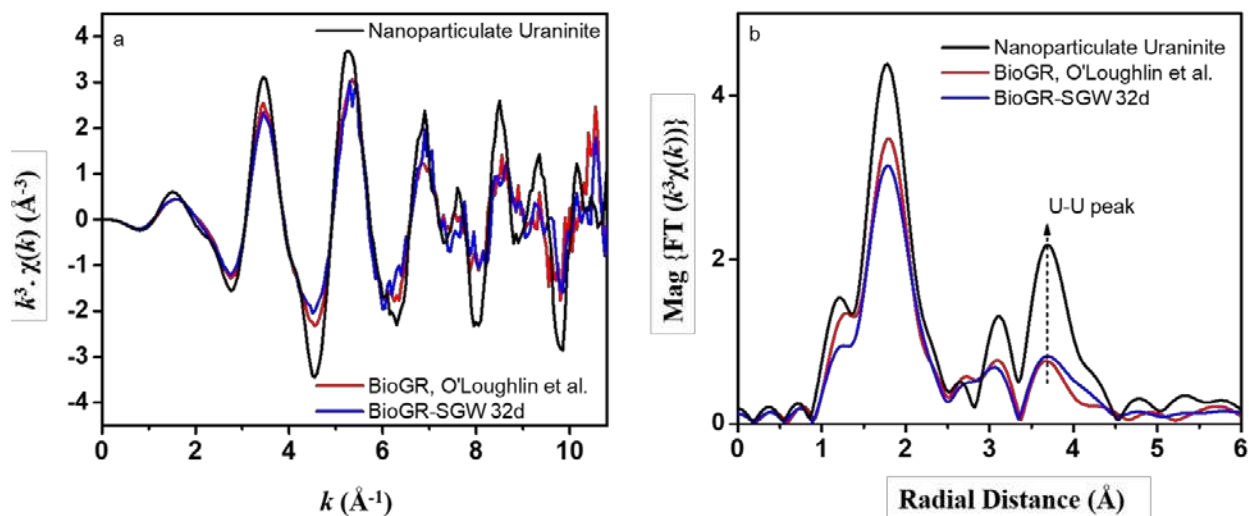


Figure S11. Comparisons between the BioGR data in this study (blue) to that in the carbonate BioGR reactor of O'Loughlin et al.⁹ (red), showing the same EXAFS data within measurement uncertainty. The data are compared to the nanoparticulate uraninite standard (black). Left: $k^3\chi(k)$ data. Right: Fourier transform between $k = 2.2 - 0.4 \text{ \AA}^{-1}$ using 1.0 \AA^{-1} Hanning windowsills.

Table S1. The relative fraction of U^{IV} species as calculated by linear combination fitting of the k^2 weighted $\chi(k)$ data using nanoparticulate uraninite and U^{IV} -carbonate standards

Sample ID/ U^{IV} Species	U^{IV} -Carbonate	Uraninite
	ChemGR in SGW	
ChemGR-SGW 1 h	92%	8%
ChemGR-SGW 32 h	75%	25%
ChemGR-SGW 32 d	23%	77%
	ChemGR in DI-water	
ChemGR-DI 1 h	76%	24%
ChemGR-DI 32 h	67%	33%
ChemGR-DI 16 d	25%	75%

Table S2. The best fit values for EXAFS modeling of a representative BioGR sample

Path	CN	Distance (Å)	σ^2 (Å ²)*10 ⁻³	E ₀ (eV)	DF	χ^2_{ν}	R-factor
Fit with the outer O shell					5.5	234	0.016
O	5.2 ± 0.4	2.35 ± 0.01	12.1 ± 1.9	-1.5 ± 0.7			
Fe	2.0 ± 0.7	3.49 ± 0.02	15.0 [#]	-1.5 ± 0.7			
O	10.0 ± 3.3	4.16 ± 0.02	16.7 ± 7.9	-1.5 ± 0.7			
Fit without the outer O shell					8.5	1335	0.072
O	5.2 ± 1.1	2.37 ± 0.02	12.4 ± 4.4	-0.4 ± 1.7			
Fe	2.7 ± 1.5	3.54 ± 0.05	15.0 [#]	-0.4 ± 1.7			

[#]The σ^2 value of the Fe shell was constrained to the same value as in Latta et al.⁸ to minimize large correlations between σ^2 and coordination number for this shell and to allow comparisons between the two studies. DF=degrees of freedom in the fit; χ^2_{ν} is the reduced chi-square of the fit; R-factor is the fractional misfit relative to the amplitude of the data. More details on these fit indicators can be found in the FEFFIT documentation.

REFERENCES:

- (1) Segre, C. U.; Leyarovska, N. E.; Chapman, L. D.; Lavender, W. M.; Plag, P. W.; King, A. S.; Kropf, A. J.; Bunker, B. A.; Kemner, K. M.; Dutta, P.; Duran, R. S.; Kaduk, J. *The MRCAT insertion device beamline at the Advanced Photon Source*, In: Pianetta, P., Arthur, J., Brennan, S., Ed. 11th US National Conference on Synchrotron Radiation Instrumentation. American Institute of Physics, New York, pp 419–422.
- (2) Latta, D. E.; Kemner, K. M.; Mishra, B.; Boyanov, M. I. Effects of calcium and phosphate on uranium(IV) oxidation: Comparison between nanoparticulate uraninite and amorphous U^{IV}-phosphate. *Geochim. Cosmochim. Acta* **2016**, *174*, 122–142.
- (3) Boyanov, M. I.; Fletcher, K. E.; Kwon, M. J.; Rui, X.; O'Loughlin, E. J.; Loffler, F. E.; Kemner, K. M. Solution and microbial controls on the formation of reduced U(IV) species. *Environ. Sci. Technol.* **2011**, *45* (19), 8336–8344.
- (4) Newville, M.; Livins, P.; Yacoby, Y.; Rehr, J. J.; Stern, E. A. Near-edge X-ray-absorption fine-structure of Pb: A comparison of theory and experiment. *Phys. Rev. B* **1993**, *47* (21), 14126–14131.
- (5) Wyckoff, R. W. G., *Crystal Structures*. 2 ed.; John Wiley & Sons: New York, 1964.
- (6) Ankudinov, A. L.; Ravel, B.; Rehr, J. J.; Conradson, S. D. Real-space multiple-scattering calculation and interpretation of X-ray-absorption near-edge structure. *Phys. Rev. B* **1998**, *58* (12), 7565–7576.
- (7) Newville, M.; Ravel, B.; Haskel, D.; Rehr, J. J.; Stern, E. A.; Yacoby, Y. Analysis of multiple-scattering XAFS data using theoretical standards. *Physica B* **1995**, *208* (1-4), 154–156.
- (8) Latta, D. E.; Boyanov, M. I.; Kemner, K. M.; O'Loughlin, E. J.; Scherer, M. Reaction of uranium(VI) with green rusts: Effect of interlayer anion. *Curr. Inorg. Chem.* **2015**, *5* (3), 156–168.
- (9) O'Loughlin, E. J.; Kelly, S. D.; Kemner, K. M. XAFS investigation of the interactions of U(VI) with secondary mineralization products from the bioreduction of Fe(III) oxides. *Environ. Sci. Technol.* **2010**, *44* (5), 1656–1661.